We are IntechOpen, the world's leading publisher of Open Access books Built by scientists, for scientists

6,900
Open access books available

185,000
International authors and editors

200M
Downloads

Our authors are among the

154
Countries delivered to

TOP 1%
most cited scientists

12.2%
Contributors from top 500 universities



WEB OF SCIENCE™

Selection of our books indexed in the Book Citation Index in Web of Science™ Core Collection (BKCI)

Interested in publishing with us?
Contact book.department@intechopen.com

Numbers displayed above are based on latest data collected.
For more information visit www.intechopen.com



Chapter 2

Electromagnetic Levitation System for Active Magnetic Bearing Wheels

Yonmook Park

Additional information is available at the end of the chapter

http://dx.doi.org/10.5772/67227

Abstract

In this chapter, the author presents an electromagnetic levitation system for active magnetic bearing wheels. This system consists of a rotor, a shaft, a cover, and a base. The author derives a meaningful electromagnetic force by using the singular value decomposition. The author develops a control system using the proportional-integral-derivative controller to control the position of the rotor and regulate the two gimbal angles of the rotor. The author gives the numerical simulation and experimental results on the control of the electromagnetic levitation system.

Keywords: active magnetic bearing, electromagnetic levitation system, motion control

1. Introduction

As a reaction wheel in spacecraft, a ball bearing wheel, a magnetic bearing wheel, and an active magnetic bearing wheel have mainly been used. First, a ball bearing wheel uses a ball bearing to maintain the separation between the bearing races. Ball bearings reduce rotational friction and support radial and axial loads by using at least two races to contain balls and transmit the loads through balls. Ball bearings tend to have a lower load capacity than other kinds of rolling element bearings mainly due to the small contact area between balls and races. Also, ball bearings should be lubricated periodically with a lubricant such as oil and grease for ball bearings to operate properly [1]. Next, a magnetic bearing is used in a magnetic bearing wheel. A magnetic bearing supports a load by the magnetic levitation principle. In magnetic bearing wheels, permanent magnets are used to carry a wheel, a control system is used to hold a wheel stable, and power is used when a levitated wheel deviates from its target position. A magnetic bearing wheel also requires a back-up bearing in case of control system or power failure and

INTECH
open science | open minds

© 2017 The Author(s). Licensee InTech. This chapter is distributed under the terms of the Creative Commons Attribution License (http://creativecommons.org/licenses/by/3.0), which permits unrestricted use, distribution, and reproduction in any medium, provided the original work is properly cited. CC BY

during initial start-up conditions. A magnetic bearing has two kinds of instabilities. One is that attractive magnets provide an unstable static force that decreases at distant distances and increases at close distances. The other is that magnetism gives rise to oscillations that may cause loss of suspension if driving forces are present [1]. Finally, in an active magnetic bearing wheel, a rotating shaft is levitated by the principle of electromagnetic suspension. A wheel is supported in an active magnetic bearing wheel without physical contact. The contactless operation of the active magnetic bearing wheels eliminates the need of lubrication of the bearing components, which allows them to operate cleanly. Moreover, it can accommodate irregularities in the mass distribution automatically, which allows it to spin around its center of mass with very low vibration, and can suppress the nutation and precession of the rotor effectively. The components of an active magnetic bearing wheel are an active magnetic bearing, a wheel, a control system, an electromagnet assembly, power amplifiers, and gap sensors. This bias current is mediated by a control system that offsets the bias current by equal but opposite perturbations of current as the rotor deviates by a small amount from its center position [1].

The active magnetic bearing wheel exhibits very lower vibration than ball bearing wheels and magnetic bearing wheels. Thus, it is a desirable reaction wheel for the spacecraft attitude control since vibration is the critical factor for the high precision spacecraft attitude control. The active magnetic bearing is the very important component among components of active magnetic bearing wheels. Due to this importance, various kinds of active magnetic bearings have been developed and their control methods have been studied (e.g., [2–10]).

In this chapter, the author presents an electromagnetic levitation system for active magnetic bearing wheels. This system consists of a rotor, a shaft, a cover, and a base. Also, this system does not include a mechanism for spinning the rotor around its rotating axis. The author derives a meaningful electromagnetic force by using the singular value decomposition [11]. The proportional-integral-derivative (PID) controller is used to control the position of the rotor and regulate the two gimbal angles of the rotor. The author gives the numerical simulation and experimental results on the control of the electromagnetic levitation system.

2. Electromagnetic levitation system

In **Figure 1**, the schematic of the electromagnetic levitation system developed in this chapter is given. The cover protects the rotor, and the base supports the rotor, shaft, and cover. This system can levitate the rotor up to 0.8 mm from the ground in the *z*-axis, rotate the rotor, and gimbal the rotor within a small angle of ±0.2°.

The dynamic equations of motion of the electromagnetic levitation system are given as follows:

$$m\ddot{z} = F_z \tag{1}$$

$$I\ddot{\phi} = T_x \tag{2}$$

$$I\ddot{\theta} = T_y \tag{3}$$

http://dx.doi.org/10.5772/67227

In Eqs. (1)–(3), ϕ and θ are the gimbal angles of the rotor in the x- and y-axes, respectively, z is the displacement of the rotor in the z-axis, F_z is the control force in the z-axis, T_x and T_y are the control torques applied to the rotor in the x- and y-axes, respectively, m = 0.72 kg is the mass of the rotor, and $I = 877.367 \times 10^{-6}$ kg m^2 is the inertia of the rotor for the x- and y-axes.

Let us consider the four pairs of electromagnets shown in **Figure 1**. Then, the control inputs F_z in Eq. (1), T_x in Eq. (2), and T_y in Eq. (3) can be represented as follows:

$$\sum_{i=1}^{4} F_{ei} = F_z + mg \tag{4}$$

$$D_e\left(F_{e2} - F_{e4}\right) = T_x \tag{5}$$

$$D_e\left(F_{e3} - F_{e1}\right) = T_y \tag{6}$$

In Eqs. (4)–(6), F_{ei} is the electromagnetic force generated by the ith pair of electromagnets, and g = 9.8 m/s^2 is the acceleration of gravity. Then, Eqs. (4)–(6) can be written as follows:

$$A F_e = u + u_g \tag{7}$$

where

$$A \triangleq \begin{bmatrix} 1 & 1 & 1 & 1 \\ 0 & D_e & 0 & -D_e \\ -D_e & 0 & D_e & 0 \end{bmatrix} \tag{8}$$

$F_e \triangleq [F_{e1}\ F_{e2}\ F_{e3}\ F_{e4}]^T$, $u \triangleq [F_z\ T_x\ T_y]^T$, and $u_g \triangleq [mg\ 0\ 0]^T$. After designing the control inputs F_z, T_x, and T_y, the four electromagnetic forces F_{ei}, i = 1,…,4 have to be determined by Eq. (7). Among solutions for Eq. (7), the minimal norm solution is derived by using the singular value decomposition [11]. Let the singular value decomposition of the matrix $A \in R^{3\times4}$ in Eq. (8) be $U\Sigma V^T$ and define

$$A^+ \triangleq V\Sigma^+ U^T \tag{9}$$

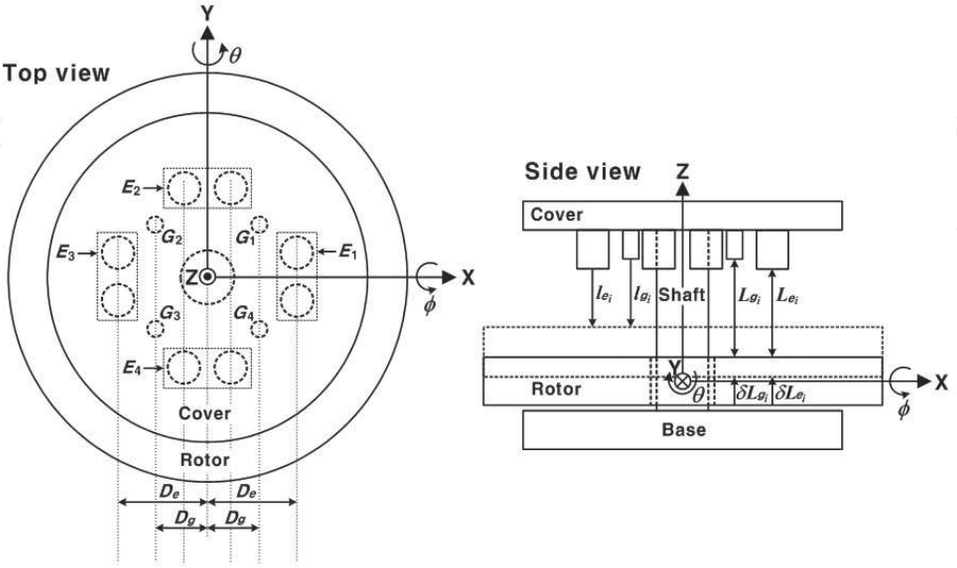


Figure 1. Schematic representation of the electromagnetic levitation system.

where $U \in R^{3\times3}$ and $V \in R^{4\times4}$ are orthogonal matrices, $\Sigma \in R^{3\times4}$, and $A^+ \in R^{4\times3}$ and $\Sigma^+ \in R^{4\times3}$ denote the pseudoinverse matrices of the matrices A and Σ, respectively. With some calculations, we obtain the following by the singular value decomposition of the matrix A in Eq. (8)

$$V = \frac{1}{2}\begin{bmatrix} 1 & 0 & -\sqrt{2} & -1 \\ 1 & \sqrt{2} & 0 & 1 \\ 1 & 0 & \sqrt{2} & -1 \\ 1 & -\sqrt{2} & 0 & 1 \end{bmatrix} \tag{10}$$

$$\Sigma^+ = \frac{1}{2}\begin{bmatrix} 1 & 0 & 0 \\ 0 & \frac{\sqrt{2}}{D_e} & 0 \\ 0 & 0 & \frac{\sqrt{2}}{D_e} \\ 0 & 0 & 0 \end{bmatrix} \triangleq \begin{bmatrix} \Sigma_1^{-1} \\ 0_{1\times3} \end{bmatrix} \tag{11}$$

$$U = \begin{bmatrix} 1 & 0 & 0 \\ 0 & 1 & 0 \\ 0 & 0 & 1 \end{bmatrix} \tag{12}$$

In Eq. (11), $0_{1\times3}$ implies the 1 × 3 zero matrix. Then, with A^+ of Eq. (9), we obtain

$$F_e = A^+\left(u + u_g\right) = \begin{bmatrix} \frac{1}{4}\left(F_z + mg\right) - \frac{1}{2}\frac{T_y}{D_e} \\ \frac{1}{4}\left(F_z + mg\right) + \frac{1}{2}\frac{T_x}{D_e} \\ \frac{1}{4}\left(F_z + mg\right) + \frac{1}{2}\frac{T_y}{D_e} \\ \frac{1}{4}\left(F_z + mg\right) - \frac{1}{2}\frac{T_x}{D_e} \end{bmatrix} \tag{13}$$

The following condition holds for any other solution $\hat{F}_e$ to Eq. (7) [12]

$$\|F_e\|_2 < \|\hat{F}_e\|_2 \tag{14}$$

where '$\|\cdot\|_2$' denotes the Euclidean norm of a vector (i.e., for a vector $x \in R^n$, $\|x\|_2 \triangleq \sqrt{\sum_{i=1}^{n} x_i^2}$).

Since the two gimbal angles, ϕ and θ, are very small, we can approximate $\sin(\phi) \cong \phi$ and $\sin(\theta) \cong \theta$ by the small-angle approximation. Thus, the displacement from the bottom surface of the ith gap sensor to the top surface of the rotor in the z-axis can be calculated as follows:

$$l_{g1} = L_{g1} + \delta L_{g1} = L_{g1} - z + D_g \sin(\theta) - D_g \sin(\phi) \cong L_{g1} - z + D_g\theta - D_g\phi \tag{15}$$

$$l_{g2} = L_{g2} + \delta L_{g2} = L_{g2} - z - D_g \sin(\theta) - D_g \sin(\phi) \cong L_{g2} - z - D_g\theta - D_g\phi \tag{16}$$

$$l_{g3} = L_{g3} + \delta L_{g3} = L_{g3} - z - D_g \sin(\theta) + D_g \sin(\phi) \cong L_{g2} - z - D_g\theta + D_g\phi \tag{17}$$

$$l_{g4} = L_{g4} + \delta L_{g4} = L_{g4} - z + D_g \sin(\theta) + D_g \sin(\phi) \cong L_{g4} - z + D_g\theta + D_g\phi \tag{18}$$

Then, from Eqs. (15) to (18), the system state z, ϕ, and θ can be calculated as follows:

$$z = \frac{1}{4}\left(\sum_{i=1}^{4} L_{gi} - \sum_{i=1}^{4} l_{gi}\right) \tag{19}$$

$$\phi = \frac{1}{4D_g}\left[\left(l_{g3} + l_{g4} - l_{g1} - l_{g2}\right) - \left(L_{g3} + L_{g4} - L_{g1} - L_{g2}\right)\right] \tag{20}$$

http://dx.doi.org/10.5772/67227

$$\theta = \frac{1}{4D_g}\left[\left(l_{g1} + l_{g4} - l_{g2} - l_{g3}\right) - \left(L_{g1} + L_{g4} - L_{g2} - L_{g3}\right)\right] \tag{21}$$

Similarly, the displacement from the bottom surface of the ith pair of electromagnets to the top surface of the rotor in the z-axis can be calculated as follows:

$$l_{e1} = L_{e1} + \delta L_{e1} = L_{e1} - z + D_e \sin(\theta) \cong L_{e1} - z + D_e \theta \tag{22}$$

$$l_{e2} = L_{e2} + \delta L_{e2} = L_{e2} - z - D_e \sin(\phi) \cong L_{e2} - z - D_e \phi \tag{23}$$

$$l_{e3} = L_{e3} + \delta L_{e3} = L_{e3} - z - D_e \sin(\theta) \cong L_{e3} - z - D_e \theta \tag{24}$$

$$l_{e4} = L_{e4} + \delta L_{e4} = L_{e4} - z + D_e \sin(\phi) \cong L_{e4} - z + D_e \phi \tag{25}$$

By the Maxwell's equation [13], the following equation is obtained for the control currents supplied to the coils of the four pairs of electromagnets

$$i_i = \frac{2l_{ei}}{n}\sqrt{\frac{F_{ei}}{\mu_0 G}},\ i = 1, \ldots, 4 \tag{26}$$

where $\mu_0 = 4\pi \times 10^{-7}$ N/A^2 is the permeability constant of free space, $n = 240$ is the number of coil turn, i_i is the control current of the ith pair of electromagnets, and $G = 50.265 \times 10^{-6}$ m^2 is the cross-sectional area of a pair of electromagnets. The author limits each control current in Eq. (26) by 1 A.

3. Numerical simulation and experimental results

The author gives the numerical simulation and experimental results on the control of the electromagnetic levitation system in this section.

The author uses the following discretized PID controller to control the displacement of the rotor in Eq. (19) and the two gimbal angles of the rotor in Eqs. (20) and (21).

$$u(t) = K_p x_e(t) + K_i T_s \sum_{i=0}^{t} x_e(i) + K_d \frac{\left(x_e(t) - x_e(t-1)\right)}{T_s} \tag{27}$$

where T_s is the sampling time and given by $T_s = 1$ ms, $x_e \triangleq x_t - x$ is the error between the system state $x \triangleq [z\ \phi\ \theta]^T$ and the target system state $x_t \triangleq [z_t\ \phi_t\ \theta_t]^T$ and $K_p \triangleq \mathrm{diag}[K_{pz}, K_{p\phi}, K_{p\theta}]$, $K_i \triangleq \mathrm{diag}[K_{iz}, K_{i\phi}, K_{i\theta}]$, and $K_d \triangleq \mathrm{diag}[K_{dz}, K_{d\phi}, K_{d\theta}]$ denote the 3 × 3 diagonal positive definite matrices.

The target position and target gimbal angles of the rotor are set to be $z_t = 0.3$ mm and $\phi_t = 0°$ and $\theta_t = 0°$, respectively. The author initially decides the feedback gains of the PID controller in Eq. (27) that can achieve the control objective by adopting the well-known Ziegler-Nichols method [14] and then finely tunes the feedback gains of the PID controller in Eq. (27) by an experiment. Also, the antiwindup compensator is used to make the overshot as small as possible. According to the Ziegler-Nichols method [14], first, $K_i = K_d = \mathrm{diag}[0, 0, 0]$ are set, and the proportional gain K_p is then increased until the system just oscillates. The proportional gain is then multiplied by 0.6, and the integral and derivative gains are calculated as $K_p = 0.6\ K_m$, $K_i = K_p(\omega_m/\pi)$, and $K_d = K_p(0.25\ \pi/\omega_m)$ where $K_m \triangleq \mathrm{diag}[K_{mz}, K_{m\phi}, K_{m\theta}]$ denotes the 3 × 3 diagonal positive definite matrix with the gain elements at which the proportional system oscillates,

and $\omega_m \triangleq \text{diag}[\omega_{mz}, \omega_{m\phi}, \omega_{m\theta}]$ denotes the 3 × 3 diagonal positive definite matrix with the oscillation frequency elements. As a result, the feedback gains of the PID controller in Eq. (27) are chosen as follows: $K_{pz} = 1000$, $K_{p\phi} = K_{p\theta} = 20$, $K_{iz} = 5000$, $K_{i\phi} = K_{i\theta} = 8.33$, $K_{dz} = 100$, and $K_{d\phi} = K_{d\theta} = 0.013$. Consequently, we see that the dominant feedback gains in this PID controller are K_p and K_i, and thus, one can obtain $K_{mz} \cong 1666.67$, $K_{m\phi} = K_{m\theta} \cong 33.33$, $\omega_m \cong 15.71$ rad/s and $\omega_{m\phi} = \omega_{m\theta} \cong 1.31$ rad/s.

The control flow diagram of the system is shown in **Figure 2**. After we measure the displacements from the bottom surfaces of the four gap sensors to the top surface of the rotor, we calculate the displacement of the rotor and the two gimbal angles of the rotor by Eqs. (19)–(21), respectively. The control input $u \triangleq [F_z \; T_x \; T_y]^T$ is made by the PID controller in Eq. (27). Then, we calculate the four electromagnetic forces and the displacements from the bottom surfaces of the four pairs of electromagnets to the top surface of the rotor by Eq. (13) and the Eq. (22)–(25), respectively. After we calculate the control currents by Eq. (26), they pass through the current limiters and are supplied to the coils of the four pairs of electromagnets by the power electronics.

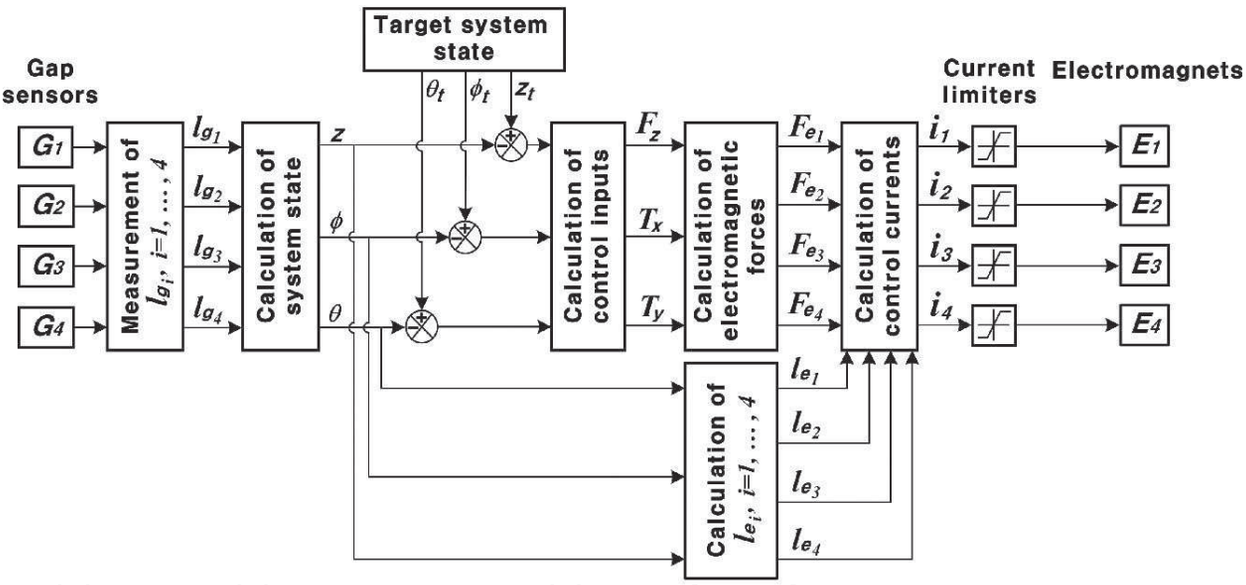


Figure 2. Control flow diagram of the electromagnetic levitation system.

In the numerical simulation, it will be demonstrated that the electromagnetic force F_e of Eq. (13) satisfies the condition of Eq. (14) with respect to the following electromagnetic force $\hat{F}_e$, which is another solution to Eq. (7)

$$\hat{F}_e = \begin{bmatrix} mg \\ \frac{1}{2}F_z + \frac{1}{2}\frac{(T_x - T_y)}{D_e} - \frac{1}{2}mg \\ \frac{T_y}{D_e} + mg \\ \frac{1}{2}F_z - \frac{1}{2}\frac{(T_x + T_y)}{D_e} - \frac{1}{2}mg \end{bmatrix} \triangleq \begin{bmatrix} \hat{F}_{e1} & \hat{F}_{e2} & \hat{F}_{e3} & \hat{F}_{e4} \end{bmatrix}^T \tag{28}$$

http://dx.doi.org/10.5772/67227

With the initial system state given by z_{ini} = 0 mm, $\dot{z}_{ini}$ = 0 mm/s, the values are $\phi_{ini} = \theta_{ini} = 0°$ and $\dot{\phi}_{ini} = \dot{\theta}_{ini} = 0°/s$. In **Figures 3–5**, the numerical simulation results on the control of the electromagnetic levitation system using F_e of Eq. (13) and $\hat{F}_e$ of Eq. (28) are shown. As shown in **Figure 3**, the rotor reaches the target position z_t = 0.3 mm, and the control forces using F_e of Eq. (13) and $\hat{F}_e$ of Eq. (28) show the same behaviors, respectively. In **Figure 4**, we see that each control current using F_e of Eq. (13) reaches the same value, the control currents of i_1 and i_3 using $\hat{F}_{e1}$ and $\hat{F}_{e3}$ of Eq. (28), respectively, reach the same value, and the control currents of i_2 and i_4 using $\hat{F}_{e2}$ and $\hat{F}_{e4}$ of Eq. (28), respectively, reach the same value. In **Figure 5**, we see that the Euclidean norm of F_e of Eq. (13) is about 3.162 times smaller than that of $\hat{F}_e$ of Eq. (28) in the steady-state region. Therefore, the numerical simulation results shown in **Figure 5** illustrate that F_e of Eq. (13) satisfies the condition of Eq. (14) with respect to $\hat{F}_e$ of Eq. (28).

The experimental results on the control of the system using F_{ei}, i = 1,…,4 of Eq. (13) are shown in **Figures 6–9**. As shown in **Figures 6** and **7**, the PID controller successfully levitates the rotor at the target position z_t = 0.3 mm with well regulating the two gimbal angles. The trajectories of control currents are shown in **Figure 8**. And the Euclidean norm of F_e of Eq. (13) is shown in **Figure 9**. As shown in **Figures 4**, **5**, **8**, and **9**, the trajectories of control currents and Euclidean norm of F_e of Eq. (13) obtained by the experiment move around the values obtained by the numerical simulation.

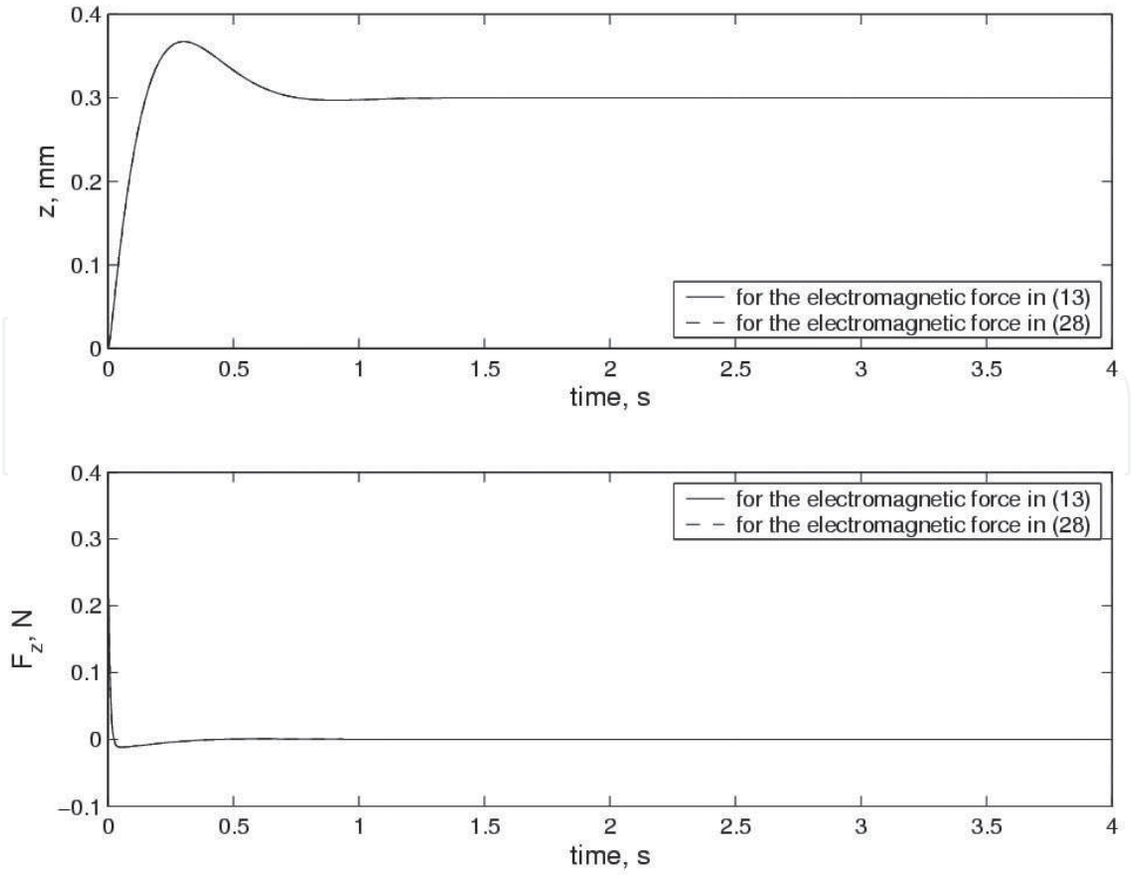


Figure 3. Time histories of the position of the rotor and the control force, which are obtained by the numerical simulation.

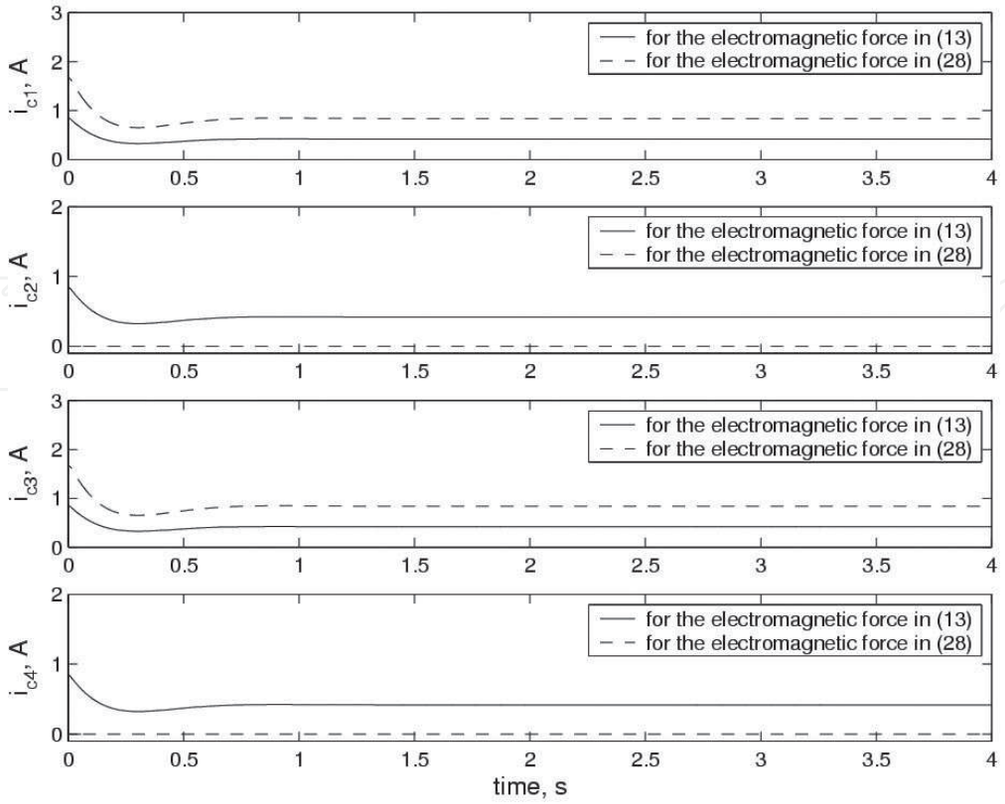


Figure 4. Time histories of the control currents, which are obtained by the numerical simulation.

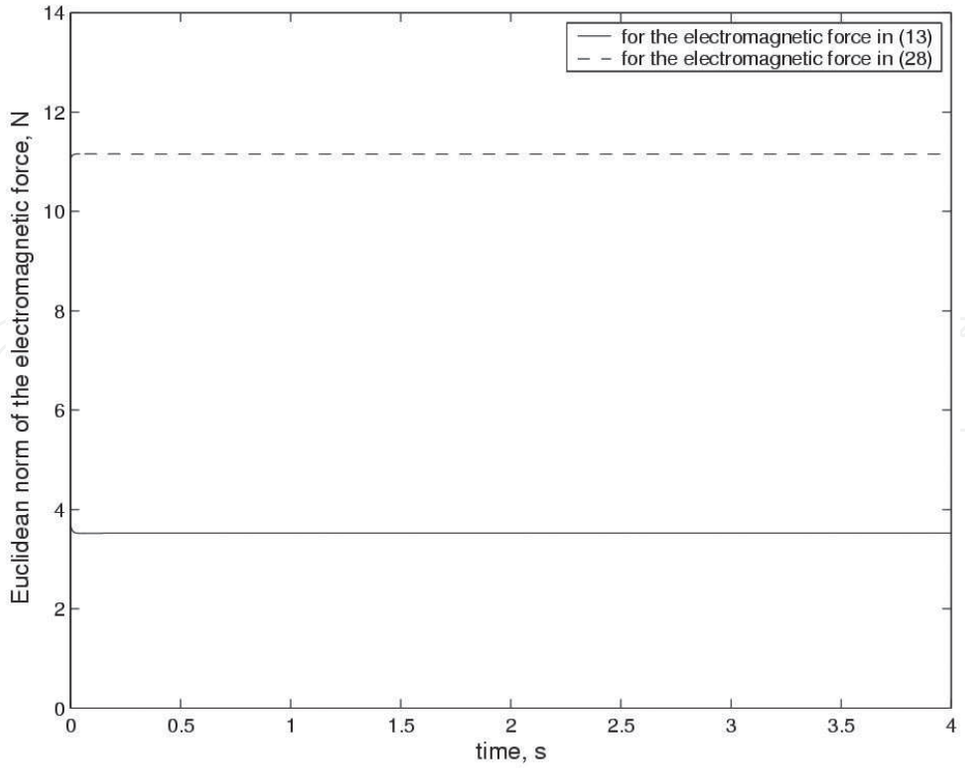


Figure 5. Time histories of the Euclidean norm of the electromagnetic force, which are obtained by the numerical simulation.

http://dx.doi.org/10.5772/67227

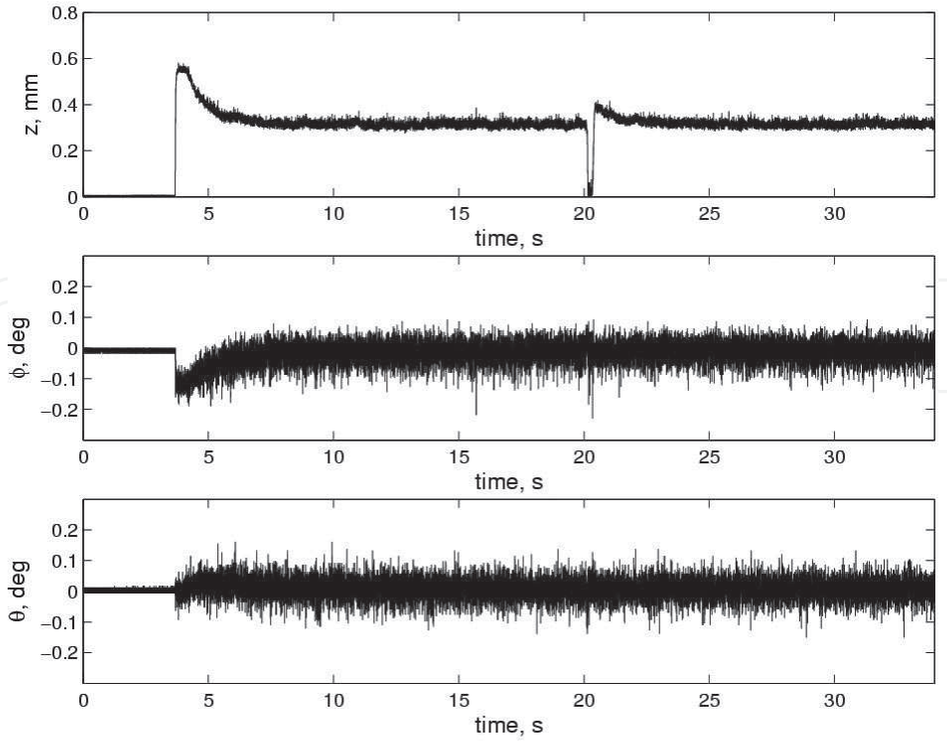


Figure 6. Time histories of the system state of the electromagnetic levitation system using Fe of Eq. (13), which are obtained by the experiment.

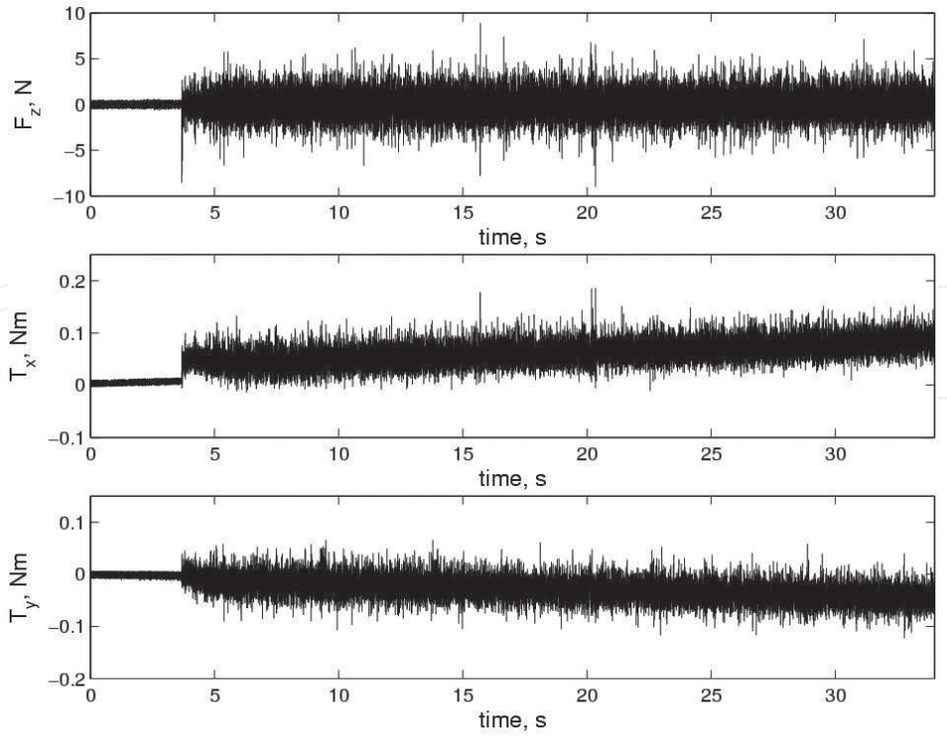


Figure 7. Time histories of the control inputs of the electromagnetic levitation system using Fe of Eq. (13), which are obtained by the experiment.

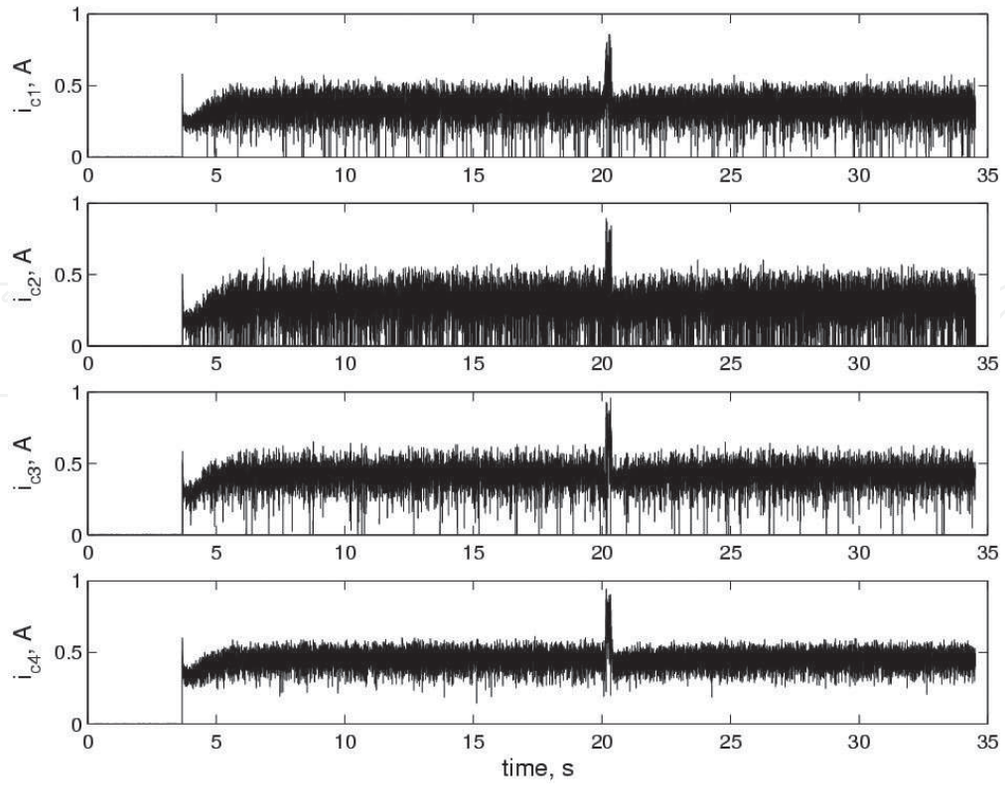


Figure 8. Time histories of the control currents of the electromagnetic levitation system using Fe of Eq. (13), which are obtained by the experiment.

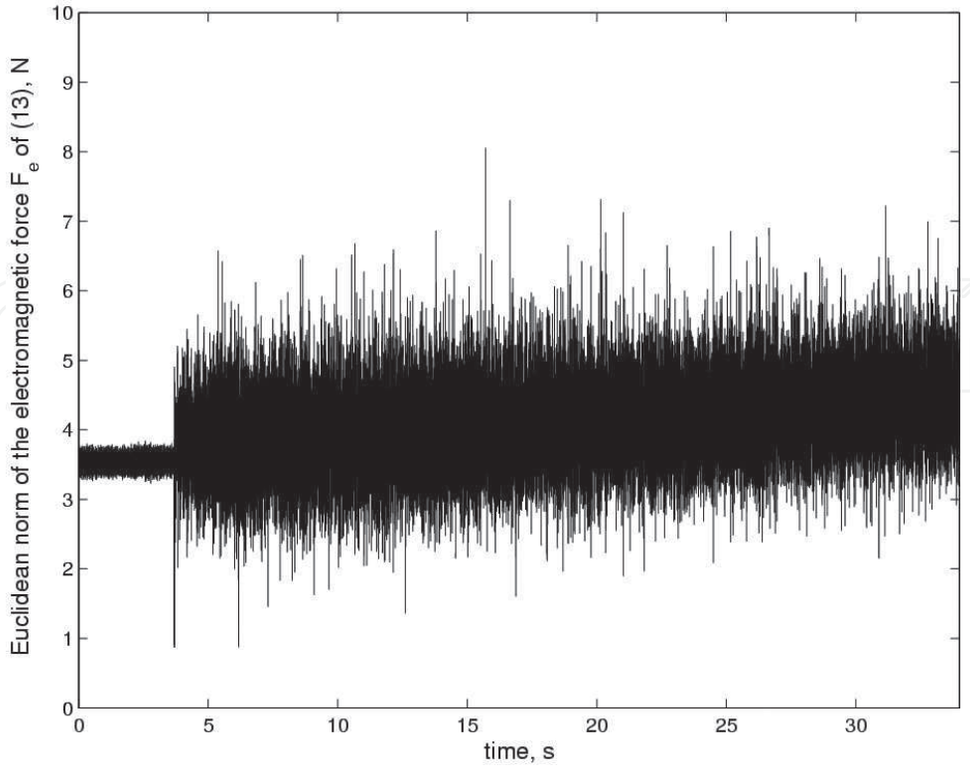


Figure 9. Time histories of the Euclidean norm of Fe of Eq. (13), which are obtained by the experiment.

In order to simulate an external disturbance, a human hand presses down hard on the rotor to the ground at about 20 s, and it is removed from the rotor momentarily. In **Figure 6**, we see that, after we remove the external disturbance from the rotor, the system state becomes a steady state within 2 s. Also, in **Figure 8**, we see that, as the external disturbance applied to the rotor increases, each control current increases to resist the external disturbance. It should be remarked that the operating parameters like an applied load and a speed of the rotor may influence on the design of electromagnetic levitation system because these parameters make an impact on the system dynamics.

4. Conclusion

In this chapter, the electromagnetic levitation system was developed as a prototype for developing active magnetic bearing wheels. A control system was developed to control the position and two gimbal angles of the rotor. The experimental results demonstrated that the control system can control the position of the rotor and regulate the two gimbal angles. The refinement of the electromagnetic levitation system for the development of active magnetic bearing wheels is the further research topic.

Acknowledgements

The author would like to thank the Satellite Technology Research Center at the Korea Advanced Institute of Science and Technology for its support to develop the electromagnetic levitation system.

Author details

Yonmook Park

Address all correspondence to: ym-park@kaist.ac.kr

Smart Machine Center, MINDs Lab. Co. Ltd., Bundang-gu, Seongnam-si, Gyeonggi-do, Republic of Korea

References

[1] Schweitzer G., Maslen E.H., editors. Magnetic bearings. Berlin, Germany: Springer; 2009. pp. 1–535.

[2] Trumper D.L., Olson S.M., Subrahmanyan P.K. Linearizing control of magnetic suspension systems. IEEE Trans. Control Syst. Technol. 1997;**5**(4):427–438.

[3] Hong S.-K., Langari R. Robust fuzzy control of a magnetic bearing system subject to harmonic disturbances. IEEE Trans. Control Syst. Technol. 2000;**8**(2):366–371.

[4] Lindlau J.D., Knospe C.R. Feedback linearization of an active magnetic bearing with voltage control. IEEE Trans. Control Syst. Technol. 2002;**10**(1):21–31.

[5] Mazenc F., de Queiroz M.S., Malisoff M., Gao F. Further results on active magnetic bearing control with input saturation. IEEE Trans. Control Syst. Technol. 2006;**14**(5):914–919.

[6] Sivrioglu S. Adaptive backstepping for switching control active magnetic bearing system with vibrating base. IET Control Theory Appl. 2007;**1**(4):1054–1059.

[7] Jugo J., Lizarraga I., Arredondo I. Nonlinear modelling and analysis of active magnetic bearing systems in the harmonic domain: a case study. IET Control Theory Appl. 2008;**2**(1):61–71.

[8] Tang J., Fang J., Wen W. Superconducting magnetic bearings and active magnetic bearings in attitude control and energy storage flywhee for spacecraft. IEEE Trans. Appl. Supercond. 2012;**22**(6):5702109.

[9] Schuhmann T., Hofmann W., Werner R. Improving operational performance of active magnetic bearings using kalman filter and state feedback control. IEEE Trans. Ind. Electron. 2012;**59**(2):821–829.

[10] Fang J., Zheng S., Han B. Attitude sensing and dynamic decoupling based on active magnetic bearing of MSDGCMG. IEEE Trans. Instrum. Meas.. 2012;**61**(2):338–348.

[11] Strang G. Linear Algebra and Its Applications. 3rd ed. Florida, USA: Harcourt Brace Jovanovich Publishers; 1988. pp. 1–505.

[12] Golub G.H., Van Loan C.F. Matrix computations. 3rd ed. Maryland, USA: The Johns Hopkins University Press; 1996. pp. 1–728.

[13] Maxwell J.C. A dynamical theory of the electromagnetic field. Phil. Trans. R. Soc. Lond. 1865;**155**:459–512.

[14] Ogata K. Modern control engineering. 5th ed. New Jersey, USA: Prentice-Hall; 1996. pp. 1–894.